Activated diffusion of benzene in NaY zeolite: Rate constants from transition state theory with dynamical corrections

Fabien Jousse
Department of Chemistry, University of Massachusetts, Amherst, Massachusetts 01003

Scott M. Auerbach[a)]
Departments of Chemistry and Chemical Engineering, University of Massachusetts, Amherst, Massachusetts 01003

(Received 15 July 1997; accepted 8 September 1997)

We calculated transition state theory and exact rate coefficients for benzene jumps in Na-Y zeolite between 150 and 500 K. This is the first exact flux correlation function rate calculation for a non-spherical molecule inside a zeolite. We calculated rates for jumps between S_{II} and W sites, located near Na ions in 6-rings and in 12-rings windows, respectively. Partition function ratios were calculated using Voter's displacement vector method. A general Arrhenius behavior is observed over the whole temperature range for all processes. The activation energies are close to the difference between the minimum energies in the sites, and between the sites and the transition states. The calculated prefactors present reasonable values around 10^{12}–10^{13} s^{-1}, in good agreement with nuclear magnetic resonance relaxation experiments. We were not able to decompose the prefactors into simple vibrational and entropic components, and therefore a complete calculation of the rate constant seems necessary to obtain reliable values. In three of the four types of motions investigated, the transition state theory rate constant is approximately equal to the more exact correlation function rate constant. However, in the case of the W→W jump, transition state theory is qualitatively wrong. This is due to the fact that the minimum energy path from one W site to another is very unstable and intersects the S_{II}→S_{II} minimum energy pathway, so a slight perturbation sends the molecule to a S_{II} site instead of the W site. As a consequence, the prefactor for the W→W jump is found to be almost one order of magnitude smaller than the prefactor for the W→ S_{II} jump, although the activation energies are similar.
[S0021-9606(97)52546-3]

I. INTRODUCTION

The sorption and diffusion of benzene in faujasite has received considerable interest in the recent years,[1–9] reflecting the importance of the catalytic processes involving aromatics in these zeolites. In a series of recent papers, Auerbach *et al.* investigated the diffusion of benzene in NaY using a kinetic Monte Carlo method (KMC),[5,6,10–13] making the first long-range simulation of diffusion in a cation containing zeolite. The nature and existence of two types of adsorption sites in NaY has been experimentally, as well as theoretically, discussed.[7,14,15] In the window site (W), the benzene molecule is stabilized by the interaction with the oxygens framing the window, while in the so-called S_{II} site the interaction with the Na_{II} sodium cation makes up for a large part of the interaction.

The high energy barriers between the sites justify the use of the KMC approach.[16] In these previous studies, the necessary transition rate constants between two sites i and j were evaluated using an Arrhenius law from the energy barrier E_{ij} between the two sites: $k_{ij}=\nu_{ij}\exp(-E_{ij}/k_BT)$, where E_{ij} were calculated by a constrained minimisation along the pathway while the prefactors ν_{ij} were set to reasonable values, e.g., 10^{13} s^{-1}.[5] The actual value of these prefactors is relatively unimportant (when all the relevant rate coefficients have roughly equal prefactors), as the temperature dependence for such high energy barriers and for reasonable temperatures stems almost exclusively from the exponential.

However, recent experiments have revealed that the prefactors might prove important. Indeed, recent deuterium solid state NMR relaxation measurements of benzene mobility in NaY, HY and USY have revealed non-Arrhenius temperature behavior of the benzene orientational randomization (BOR) rate in HY and USY, but normal Arrhenius dependence in NaY.[8] The authors attribute the non-Arrhenius behavior to competition between intracage (S_{II}→S_{II}) and intercage (S_{II}→W) processes, which supposes different activation energy for these two processes, but also very different preexponential factors. The prefactor for the S_{II}→S_{II} and S_{II}→W processes were estimated from the NMR results to ca. 10^9 s^{-1} and 10^{12} s^{-1}, respectively. The three orders of magnitude difference between these two processes is very atypical. Hence, there is a great interest in predicting reliable prefactors for the inter- and intracage processes in these materials.

Transition state theory (TST) and correlation function theory have been used successfully to compute the rate constants for the diffusion of adatoms on surfaces[17–20] and also for a number of sorbate molecules in zeolitic systems.[9,16,21] To our knowledge there is no report in the literature of exact

a)Author to whom all correspondence should be addressed.

rate coefficient calculations of non-spherically symmetric molecules in zeolites, and only few studies of approximate rate constants for such systems.[9,22–24] Such an accurate rate calculation is crucial for making reliable comparisons with the NMR data of Gladden and co-workers.[8]

We concentrate in this paper on determining the TST and dynamically corrected rate constants of benzene in the model of NaY (Si:Al=2.0) used in a previous study by Auerbach *et al.*,[5] using a fixed zeolitic framework. In spite of the simplicity of the model, many long computations are needed to obtain statistically meaningful results. Furthermore, the presence of cations in the structure makes compulsory the calculation of long range Coulombic interactions between benzene and the zeolite, which can be very expensive in terms of computing time. A special implementation of the fast multipole method[25] (FMM) was employed in this work, significantly speeding the electrostatic computation as compared to the standard Ewald method. The computational procedure described below thus allows challenging calculations to be performed in quite reasonable amounts of CPU time.

In three of the four types of motions investigated, the transition state theory rate constant turns out to be very close to the more exact correlation function rate constant. However, in the case of the W→W jump, TST is qualitatively wrong. We will discuss the source of this error below. The rest of this paper is organised as follows: the following section describes the methods used in the calculation; the third section gives some tests and justifications of these methods, the fourth section presents the results and a discussion of our findings, and the fifth section gives concluding remarks.

II. METHODS

A. Force field and model

The potential energy surface used in this paper has been described previously[5,6] and will not be detailed here. The zeolite-guest interactions consists of a Lennard-Jones 6–12 potential plus long-range Coulombic interactions using partial charges on both the zeolite and guest atoms; guest intramolecular interactions are described by a valence force field including a harmonic bond, a harmonic angle, and a torsion angle term. The Coulombic interactions were computed using a fast multipole method (FMM);[25] the speed of the FMM method indeed competes successfully with Ewald calculations, in the particular case of the interaction between a sorbed molecule and a fixed lattice.

In the fast multipole method the Coulombic energy between the ions located in two distinct regions of space A and B is written as an infinite sum over the multipole moments in the regions A and B:

$$\phi_{AB}=\sum_{l=0}^{\infty}\sum_{m=-l}^{l}\mu_{lm}^{A}(Q^{A},\mathrm{R}^{A})\,\omega_{lm}^{B}(Q^{B},\mathrm{R}^{B}), \tag{1}$$

where we assumed $\forall \mathbf{r}_i \in A, \forall \mathbf{r}_j \in B$, $|\mathbf{r}_i|>|\mathbf{r}_j|$, and we have defined:

$$\mu_{lm}^{A}(Q^{A},\mathrm{R}^{A})=\sum_{i\in A} q_i \mathscr{I}_{lm}(\mathbf{r}_i)$$
$$\omega_{lm}^{B}(Q^{B},\mathrm{R}^{B})=\sum_{j\in B} q_j \mathscr{R}_{lm}(\mathbf{r}_j) \tag{2}$$

with $\mathscr{I}_{lm}(\mathbf{r})$ and $\mathscr{R}_{lm}(\mathbf{r})$ denoting solid harmonics:[26,27]

$$\mathscr{I}_{lm}(\mathbf{r})=(l-m)!\,r^{-l-1}P_{lm}(\cos\theta)\mathrm{e}^{-\mathrm{i}m\phi}$$
$$\mathscr{R}_{lm}(\mathbf{r})=\frac{1}{(l+m)!}r^{l}P_{lm}(\cos\theta)\mathrm{e}^{\mathrm{i}m\phi}. \tag{3}$$

The FMM uses the fact that if the subsets A and B are sufficiently far apart, the infinite sum in equation 1 can be truncated at only a few terms. More precisely, the simulation cell and its periodic replicas are divided into smaller regions by cutting them in two along each axis of the cell, each of these smaller regions being themselves divided into smaller parts. The ''sufficiently far apart'' criterion then requires than each region be separated by two regions or more, and thus has a different meaning for each division level.

In the general case, the computation of $\mu_{lm}^{A}(Q,\mathrm{R})$ and $\omega_{lm}^{B}(Q,\mathrm{R})$ requires a large computational effort, so that computing the electrostatic energy with the fast multipole method becomes more rapid than the Ewald method only for thousands of atoms or more.[26–29] However, in the special case of the interaction between a guest molecule and the zeolite lattice, all coefficients μ_{lm} and ω_{lm} pertaining to the lattice can be precomputed and stored, so that the calculation becomes very fast. To a comparable relative accuracy of $\approx 10^{-6}$ the FMM calculation was found to be significantly faster than the direct Ewald summation.

The simulation cell consisted of 652 particles (640 zeolite atoms and 12 benzene atoms) under periodic boundary conditions. The Si/Al ratio of 2.0 requires 64 Na atoms in the simulation cell, assumed to fully occupy the I' sites in the β cages and the II sites in the supercages. As noted before, the zeolite atoms and Na ions were held fixed during all simulations presented here.

B. Calculation of the rate constants

The approach used in this paper follows closely the formulation of transition state theory with dynamical corrections as formulated by Voter and Doll[19] from a theory first presented by Chandler.[30]

The flux correlation function rate constant for the jump from an original site i to a final site j can be expressed as:

$$k_{i\to j}(t)=\frac{1}{\chi_i}\langle \dot{\zeta}(0)\,\delta_i[\mathbf{r}(0)]\Theta_j[\mathbf{r}(t)]\rangle, \tag{4}$$

where χ_i is the equilibrium mole fraction of particles in the state i, ζ the particle coordinate perpendicular to the dividing surface bounding state i, $\delta_i[\mathbf{r}]$ denotes the Dirac delta function $\delta[\mathbf{r}-\mathbf{r}_i^{\ddagger}]$ whose value is 1 if the particle lies on the boundary surface of state i, and $\Theta_j[\mathbf{r}]$ is the standard step function whose value is 1 if the particle is in state j and zero otherwise.

Equation 4 represents the flux of particles flowing through the dividing surface at time 0, weighted by the step function indicating that only those molecules that are in the site j at time t are counted in the average. $k_{i\to j}$ is seen to depend explicitly on time t; the physically meaningful rate constant should be evaluated from equation 4 for a time t such that $\tau_{\rm corr} < t \ll \tau_{\rm rxn}$, where $\tau_{\rm corr}$ is the typical time of the vibrational motion of the particle in its site and $\tau_{\rm rxn}$ is the typical time between two ''reactive'' events. It is important that the final result does not depend, in principle, on the choice of dividing surface.

The standard transition state rate coefficient can be written in the same notation:

$$k_{i\to j}^{\rm TST} = \frac{1}{\chi_i} \langle \dot{\zeta}(0)\, \delta_i[\mathbf{r}(0)] \Theta_j[\mathbf{r}(\epsilon)] \rangle, \tag{5}$$

where ϵ is a very short time. Unlike equation 4, here all trajectories which leave site i and enter site j at time 0 are considered reactive; therefore, equation 5 strongly depends on the exact position of the transition state. The last equation can be rewritten in the usual form:

$$k_{i\to j}^{\rm TST} = \frac{1}{2}\left(\frac{2k_{\rm B}T}{\pi m}\right)^{1/2} \frac{Q^{\ddagger}}{Q_i}, \tag{6}$$

where $Q^{\ddagger}$ is the partition function in the transition state and Q_i the partition function in the reactant state i. The last expression can be evaluated by a Monte Carlo simulation with relative ease. The exact rate constant can then be written as:

$$k_{i\to j} = k_{i\to j}^{\rm TST} \times f_{ij}(t), \tag{7}$$

where the so-called dynamical correction factor is:

$$f_{ij}(t) = \frac{\langle \dot{\zeta}(0)\, \delta_i[\mathbf{r}(0)] \Theta_j[\mathbf{r}(t)] \rangle}{\langle \dot{\zeta}(0)\, \delta_i[\mathbf{r}(0)] \Theta_j[\mathbf{r}(\epsilon)] \rangle}. \tag{8}$$

The dynamical correction factor is usually evaluated from short molecular dynamics simulations originating on the dividing surface. While equations 6 to 8 are standard expressions of transition state theory and correlation function theory, the exact way in which they are implemented depends strongly upon the actual system of interest. Indeed, if the transition state dividing surface is precisely known (as for the case of an adatom), equation 6 then provides a good first approximation to the rate constant, and the dynamical correction factor accounts for the possibility that the particle does not thermalize in the state it has first reached, but instead goes on to a different final state. This process is called ''dynamical recrossing'' if the final state is identical to the original state, and otherwise is called ''multisite jumping.'' The importance of dynamical recrossing or multisite jumping depends on a number of factors, of which the height of the energy barriers and the mechanism of energy dissipation are essential. More important, perhaps, is the fact that the rate constant computed via equation 6 does not depend on the exact location of the transition state, as long as the dynamical correction factor $f_{ij}(t)$ can be evaluated with enough accuracy.

In a complex system with many degrees of freedom it might be difficult, or even impossible, to define rigorously the dividing surface between the states. In this case the transition state approximation may fail, and the use of equation 6, or of an equivalent expression based on a similar correlation function theory becomes compulsory. Indeed, transition state theory assumes that all trajectories initially crossing the dividing surface in the direction of the product state will eventually relax in this state. This statement will be qualitatively false if the supposed surface does not coincide with the actual dividing surface. In this case, flux correlation function theory corrects TST for an inaccurately defined dividing surface.

The two steps of the calculation, namely, the calculation of the ratio of the partition functions (equation 7) and the dynamical correction factor (equation 8), are described in the next two subsections.

1. Ratio of the partition functions

The calculation of partition functions is notoriously difficult, and a number of methods have been proposed and implemented.[31–34] However, for most of these methods, the application to a non spherically symmetric system such as benzene is far from straightforward. We selected and implemented the displacement vector method proposed by Voter.[31]

In this method the ratio of the partition function between two regions of phase space A and B is computed from the following equation:

$$\frac{Q_B}{Q_A} = \frac{\langle M_\beta[V_B(\mathbf{r}+\mathbf{d}) - V_A(\mathbf{r})] \rangle_A}{\langle M_\beta[V_A(\mathbf{r}-\mathbf{d}) - V_B(\mathbf{r})] \rangle_B}, \tag{9}$$

where $M_\beta(\Delta E) = \min(1, \exp(-\beta \Delta E))$ designs the usual Metropolis sampling function in the canonical ensemble. The term $\langle M_\beta[V_B(\mathbf{r}+\mathbf{d}) - V_A(\mathbf{r})] \rangle_A$ ($\langle M_\beta[V_A(\mathbf{r}-\mathbf{d}) - V_B(\mathbf{r})] \rangle_B$, respectively) in equation 9 is simply the Monte Carlo average over state A (B, respectively) that a fictitious move from A to B (B to A, respectively) with the displacement vector $\mathbf{d}$ should be accepted.[31]

Equation 9 can be used to determine the ratio of the partition functions $Q^{\ddagger}/Q_i$ of equation 6 by setting:

$$\frac{Q^{\ddagger}}{Q_i} = \lim_{\epsilon \to 0} \frac{Q_B^{\epsilon}}{Q_A} \tag{10}$$

with:

$$V_A(\mathbf{r}) = \begin{cases} V(\mathbf{r}) & \mathbf{r} \in \text{state } i \\ \infty & \mathbf{r} \notin \text{state } i \end{cases}, \tag{11}$$

$$V_B^{\epsilon}(\mathbf{r}) = \begin{cases} V(\mathbf{r}) & \mathbf{r} \in [\mathbf{r}^{\ddagger} - \boldsymbol{\epsilon}, \mathbf{r}^{\ddagger} + \boldsymbol{\epsilon}] \\ \infty & \mathbf{r} \notin [\mathbf{r}^{\ddagger} - \boldsymbol{\epsilon}, \mathbf{r}^{\ddagger} + \boldsymbol{\epsilon}] \end{cases}, \tag{12}$$

where ϵ represents a very small width associated with the transition state, used for practical implementation, and $\mathbf{r}^{\ddagger}$ denotes the coordinates of the dividing surface. The displacement vector should be a 6-dimensional vector connecting the minimum free energy position in the reactant state and the transition state, since in our case the orientation of the molecule is important.

Two important features, proposed in the original work of Voter, facilitate the actual computation for a transition state rate constant.

- The use of a bias potential V_{bias}, approximately equal to the difference between the minimum energy in the reactant site and in the transition state, lowers the minimum energy in the transition state to values close to that in the reactant state. Let us denote C the new ''artificial'' state whose energy is now $V_C(\mathbf{r}) = V_B(\mathbf{r}) + V_{\text{bias}}$. Then equation 9 becomes:

$$\frac{Q^{\ddagger}}{Q_i} = \exp[-\beta V_{\text{bias}}] \frac{\langle M_\beta [V_C(\mathbf{r}+\mathbf{d}) - V_A(\mathbf{r})] \rangle_A}{\langle M_\beta [V_A(\mathbf{r}-\mathbf{d}) - V_C(\mathbf{r})] \rangle_C}. \tag{13}$$

- We used, instead of a single displacement vector **d** connecting the reactant state to the transition state, a distribution of vectors. This distribution is sampled during the Monte Carlo average. In theory, any distribution for **d** should lead to the same exact result, provided that the run is long enough. In practice, its size has to be adapted so as to speed up the convergence. We used throughout a Gaussian dispersion with a half-width of 0.8 Å for the translational displacement vector. It has been shown previously[5] that the orientation of the benzene molecule is rather free at the transition state between two S_{II} sites; therefore, the dispersion of the orientational displacement vector has to be large to account for all possible orientations on the dividing surface. We chose to model this large dispersion by a complete randomization of the orientational displacement vector.

2. Dynamical correction factor

The dynamical correction factor of equation 8 can be computed by a canonical average over molecular dynamic runs originating in the transition state.[19] The Monte Carlo sampling in the transition state provides us with initial conditions for the molecular positions; the atomic velocities are set according to a Boltzmann distribution at the desired temperature. At a given time t, let us note $S_P(t)$ the set of the initial N trajectories that are in the product state. Then the numerator in equation 8 is:

$$\langle \dot{\zeta}(0)\, \delta_i[\mathbf{r}(0)]\, \Theta_j[\mathbf{r}(t)] \rangle = \frac{1}{N} \sum_{i \in S_P(t)} \dot{\zeta}(0). \tag{14}$$

Since the transition state theory assumes that all trajectories with initial velocity $\dot{\zeta}(0)$ positive are reactive, the denominator of equation 8 is evaluated as:

$$\langle \dot{\zeta}(0)\, \delta_i[\mathbf{r}(0)]\, \Theta_j[\mathbf{r}(\epsilon)] \rangle = \frac{1}{N} \sum_{i | \dot{\zeta}(0) > 0} \dot{\zeta}(0). \tag{15}$$

The typical behavior of $f_{ij}(t)$ has been illustrated a number of times. Starting at 1 for $t=0$, $f_{ij}(t)$ reaches a plateau for times t such as $\tau_{\text{corr}} < t \ll \tau_{\text{rxn}}$, and finally decreases to zero for times larger than τ_{rxn}; the dynamical factor used to correct the rate constant is the plateau value. Obviously, in the general case it is not necessary for the run to last longer than the time required to reach the plateau.

The dynamical factor corrects for two problems of TST: the dynamical recrossings and multiple jumps, and also the uncertain definition of the transition state. The diffusion of benzene in NaY involves energy barriers larger than 0.35 eV, while we typically investigate temperatures ranging between 100 and 500 K, so that $0.0086 < kT < 0.043$ eV. Rapid thermalization of benzene is ensured by redistribution of the kinetic energy in the internal degrees of freedom. Therefore, dynamical recrossings and multisite jumps are likely to be of minor importance. On the other hand, a precise definition of the dividing surface between the states is very difficult to achieve. It is expected then that the dynamical factor will essentially correct for the incomplete knowledge of the dividing surface position.

This remark allows us to simplify the molecular dynamics procedure used to get $f_{ij}(t)$: indeed, once the molecule has reached the ''bottom'' of a given state, it is very unlikely that it will leave this state, and the MD run can then be aborted. Therefore, all MD runs initiated at the transition state were run only until one of the stable in the cavity is reached, defined by the position of the benzene center of mass. The subset $S_P(t)$ used in equation 14 is then composed of those trajectories which ended in the product state. A typical trajectory lasted less than 2000 fs, which allows us to perform as many as 2000 MD runs for one calculation.

3. Molecular dynamics

In addition to the MD runs performed to compute $f_{ij}(t)$, a small number of runs were initiated at a window site and at a S_{II} site, in order to investigate the short-time motions of benzene at a site. All these runs were performed in the NVE ensemble and lasted 200 ps with a 1 fs timestep. Velocities were initialized within a Maxwell-Boltzmann distribution at 600 K and the system was equilibrated for 20 000 steps before starting to accumulate data. Since the initial systems corresponded to minimum energy conformations, redistribution of the energy resulted in a mean temperature close to 300 K. The main results of these runs are the center-of-mass velocity autocorrelation function and the orientational autocorrelation function (VACF and OCF, respectively), providing information about the short-time vibrations and librations of the molecule at its site:[35]

$$\text{VACF}(t) = \frac{\langle \mathbf{v}(t) \cdot \mathbf{v}(0) \rangle}{\langle \mathbf{v}(0) \cdot \mathbf{v}(0) \rangle}, \tag{16}$$

$$\text{OCF}(t) = \frac{\langle \mathbf{n}(t) \cdot \mathbf{n}(0) \rangle}{\langle \mathbf{n}(0) \cdot \mathbf{n}(0) \rangle}, \tag{17}$$

where **v** is the velocity of the molecular center-of-mass and **n** is the normal vector associated with the benzene plane. The Fourier Transform of these quantities give the vibrational and orientational density of states (VDOS and ODOS, respectively).

C. Sites and transition states

The minimum energy sites, and the exact location of the transition states between them were found in a previous

TABLE I. Activation energies and preexponential factors for the diffusion of benzene in a model NaY(Si:AL =2.0). Activation energies from minimisation were computed in Reference 5. The activation energies and the preexponential factors from TST and correlation functions were estimated from a linear fit of $\ln k$ vs $1/T$.

	Activation energy (kJ mol^{-1})			Arrhenius prefactors	
	Minimisation	TST	Corr. function	TST	Corr. function
$W \rightarrow S_{II}$	16	17.0 ± 0.1	16.4 ± 0.3	2.7×10^{12} s^{-1}	1.1×10^{12} s^{-1}
$W \rightarrow W$	18	–	15.1 ± 4.0	–	2.4×10^{11} s^{-1}
$S_{II} \rightarrow W$	41	44.8 ± 0.1	44.4 ± 0.1	1.6×10^{13} s^{-1}	0.8×10^{13} s^{-1}
$S_{II} \rightarrow S_{II}$[a]	35	37.4 ± 0.1	36.8 ± 0.3	1.6×10^{13} s^{-1}	0.8×10^{13} s^{-1}
$S_{II} \rightarrow S_{II}$[b]	35	36.7 ± 0.1	36.9 ± 0.2	1.4×10^{13} s^{-1}	0.9×10^{13} s^{-1}
$\kappa^0(S_{II} \rightarrow W)$	25	28.0 ± 0.2		7.1	

[a]Transition state no. 1 in the middle of the $S_{II} \rightarrow S_{II}$ path.
[b]Transition state no. 2 displaced by 0.3 Å toward the product state.

study using the same forcefield and model.[5,6] A molecular dynamics docking procedure allowed the determination of sites while a constrained minimisation was used to find the minimum energy path (MEP) between the sites, and therefore the energy barriers; these in turn have been used as a first approximation to determine the rate constants (see Refs. 5 and 6). Two minimum energy sites were found, in accordance with experiment: the S_{II} site, in which the benzene molecule coordinates facially to the Na(II) cation, with a binding energy of 75 kJ mol^{-1}; in the window (W) site, the binding energy is smaller: ca. 50 kJ mol^{-1}. The height of the energy barrier determined from the constrained dynamics calculation are given in Table I; details of the calculations can be found elsewhere.[5] One zeolite supercage contains four S_{II} sites and four W sites (shared between two supercages), building a tetrahedral frame shown in Figure 1.

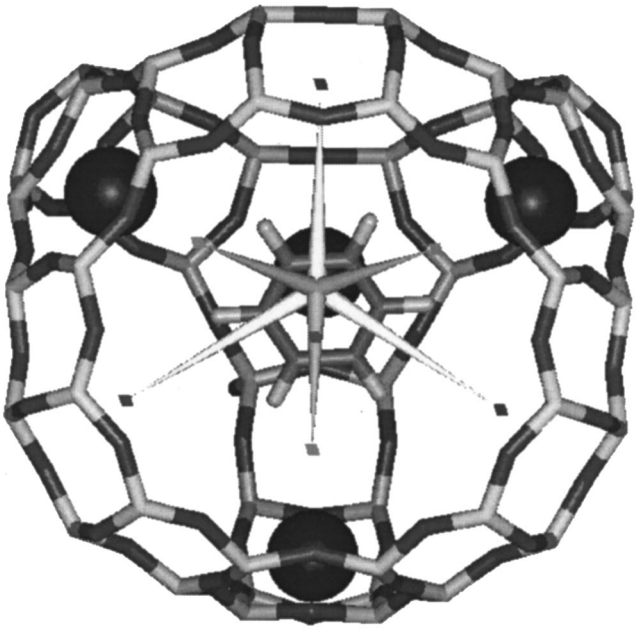

FIG. 1. Arrangement of the 4 S_{II} and W sites in a supercage of a model zeolite Na-Y with Si/Al = 2.0. The lines join the S_{II} site ''containing'' the benzene molecule to the three neighboring S_{II} sites and the three neighboring W sites.

The Monte Carlo determination of the rate constants requires knowledge not only of the transition state but also of the dividing surface between the reactant and product states. As indicated in the previous section, computing the dynamical factor makes up for the imperfection of the definition of the dividing surface, so that what we really need is only a good first order approximation. The symmetry of the supercage (when the framework atoms are held fixed) helps finding this first order approximation.

A site is defined as the region of space surrounded by the dividing surfaces for all the possible jumps out of that site. For a given jump, the dividing surface is a plane bounded by the dividing surface for all other jumps. This simple approximation gives the dividing surfaces whose projection along a schematic S_{II}-S_{II}-W-W plane is sketched in Figure 2. It is justified by a number of features of the actual sites: (i) the symmetry of the $S_{II} \rightarrow S_{II}$ path (and of the $W \rightarrow W$ path) requires the corresponding dividing surface to be on the symmetry plane; (ii) the transition state for the $S_{II} \rightarrow W$ jump lies on the line joining the S_{II} and the W sites.

A problem appears for the $W \rightarrow W$ jump: the dividing surface is indeed reduced to naught by the $W \rightarrow S_{II}$ dividing planes (see Figure 2). Of course this does not mean that there is actually no dividing surface, but only that it cannot be defined in as simple and logical a way as for the $S_{II} \rightarrow S_{II}$ and $S_{II} \rightarrow W$ processes. Boundaries were placed on the W–W

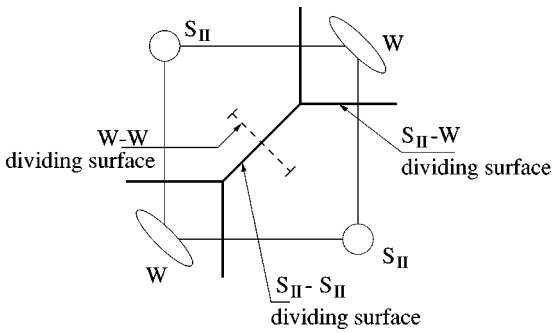

FIG. 2. Sketch of the projection on a plane containing two S_{II} and two W sites of the dividing surfaces between the S_{II} and W sites. The dividing surface used to calculate the $W \rightarrow W$ rate constant is indicated with dashed lines.

symmetric plane on each side in the middle 4-ring, so that its total extent amounts to 2.4 Å (see Figure 2). Indeed, to extend the boundary surface would cause it to get close to the S_{II} site, which is obviously not a possible transition state for the W→W jump.

Note that the actual positions of the W and S_{II} sites used in the calculation are not the minimum energy positions but the average positions over the MD runs in these sites at 298 K. These sites are close to but slightly different from minimum energy positions: in contrast to the minimum energy S_{II} sites, the average S_{II} sites are located on the line joining the Na(II) cation to the center of the cavity, and thus there is a unique site per cation.

III. TESTS OF THE METHODS

The high symmetry of the $S_{II}\rightarrow S_{II}$ path makes it a perfect candidate for testing our method of rate constant calculation. Three tests have been performed and are presented in this section: (i) the convergence of k^{TST} and k^{CF} with respect to the ''width'' ϵ of the transition state; (ii) the dependence of k^{TST} but the independence of k^{CF} with respect to the definition of the transition state; and (iii) the equivalence between a complete correlation function calculation and our truncated implementation stopping as soon as the molecule reaches a site.

1. The transition state rate constants for the $S_{II}\rightarrow S_{II}$ jump at 298 K were evaluated from the average over 200 000 Monte Carlo steps in both the reactant and the transition state, using a bias potential of -0.37 eV. The dynamical correction factors were calculated from the average over 2 000 MD trajectories initialized at the transition state, using the truncated implementation. Statistical errors in all cases were estimated from the 95% confidence interval on the value of the average; these statistical errors provide the error bars (see Figures 4, 6, and 10). The excellent convergence of the dynamical correction factor with as few as 2000 runs is exemplified by Figure 3, for a $S_{II}\rightarrow S_{II}$ process at 298 K.

The $S_{II}\rightarrow S_{II}$ rate constants were calculated at 298 K for six different widths ϵ of the dividing surface, between 0.1 and 0.8 Å. Both the transition state theory and the correlation function theory rate constants remained constant for all widths: a small rise that seems to occur toward very thin width $\epsilon<0.1$ Å is not statistically significant, and therefore in all further studies a uniform width $\epsilon=0.2$ Å was assumed.

2. By definition, k^{CF} should be independent of the exact definition of the transition state, while k^{TST} is strongly dependent. This fact has been often touched upon but rarely verified. Since it forms the core of our current calculation (and the basics for flexible framework calculation, where the TS can hardly be defined), an actual verification seems necessary. To study this dependency, we used an alternate definition of the $S_{II}\rightarrow S_{II}$ dividing surface, slightly displaced by 0.3 Å toward the product state.

The parameters of the runs were identical to the ones used to study the dependence of k with ϵ given above, both for transition state theory and correlation function theory. Figures 4a and b present the resulting rate constants, for the

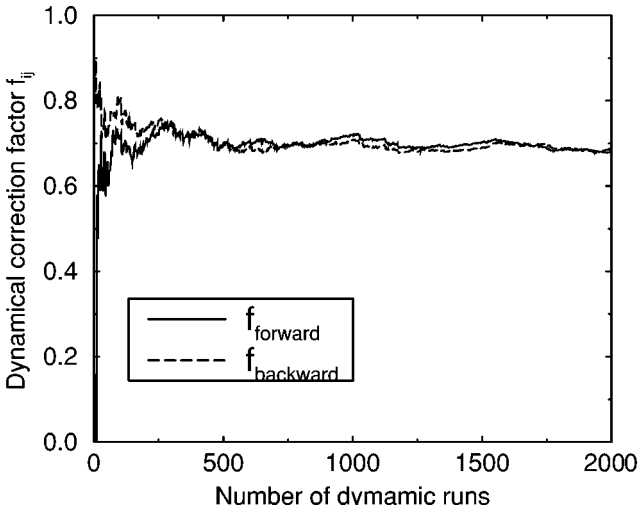

FIG. 3. Convergence of the dynamical correction factor for a $S_{II}\rightarrow S_{II}$ jump at 298 K, as a function of the number of molecular dynamics runs used in the average. $f_{forward}$ (solid line) represents the reactive event, where the molecule end in the product state; $f_{backward}$ (dotted line) represents the jump back to the original reactant state.

''real'' and ''misplaced'' transition states (noted TS 1 and TS 2, respectively), calculated from TST and TST with dynamical corrections. Figure 4a presents the raw results, while all data on Figure 4b have been multiplied by

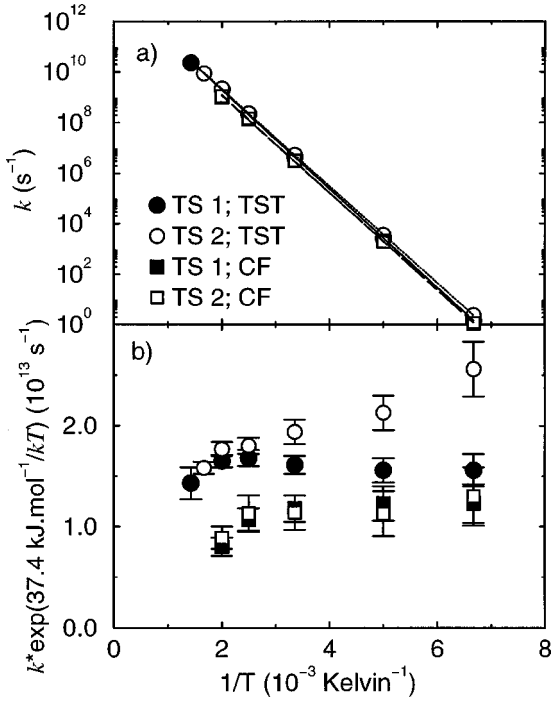

FIG. 4. Plot of the rate constants for a $S_{II}\rightarrow S_{II}$ jump, using transition state theory (TST) and correlation function theory (CF). The filled symbols (marked TS 1) are data computed using the best first order guess to the transition state dividing surface depicted in Figure 2, while the open symbols (marked TS 2) correspond to data computed using a dividing surface displaced by 0.3 Å toward the product state. (a) raw data $k(S_{II}\rightarrow S_{II})$; (b) data compensated for the apparent Arrhenius behavior $k(S_{II}\rightarrow S_{II})\times\exp(37.4\text{eV}/kT)$.

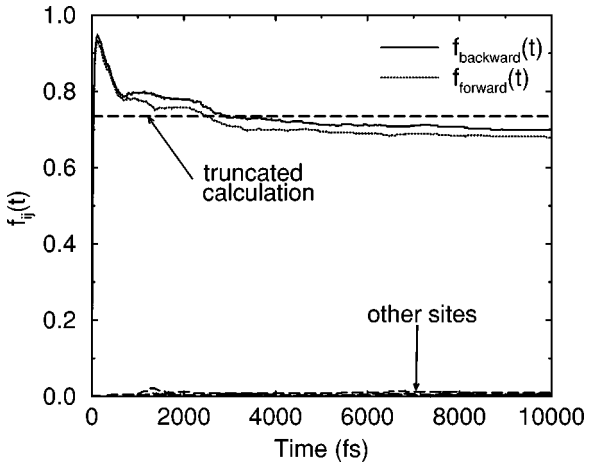

FIG. 5. Dynamical correction factor $f_{ij}(t)$ for the $S_{II} \rightarrow S_{II}$ jump, computed from the average over 2000 10 ps molecular dynamic trajectories originating at the transition state. $f_{ij}(t)$ is defined by equation 8. Solid line: i = reactant; j = reactant (backward). Dotted line: i = reactant; j = product (forward). Other: $i=$ reactant; $j=$ other products. Note the dashed line corresponding to the result of a truncated calculation, as described in Sec. II B.

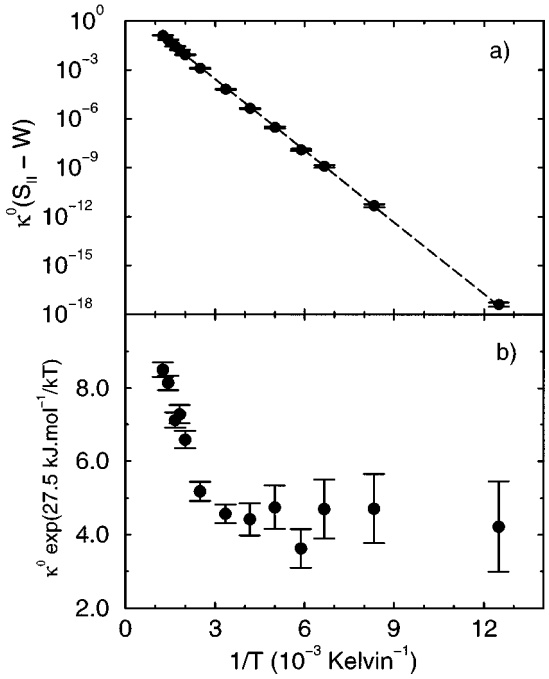

FIG. 6. Chemical Equilibrium Constant $\kappa^0(S_{II} \rightarrow W)$, as computed with the displacement vector method over 200 000 Monte Carlo steps. (a): raw data; (b): data compensated for the energy difference between the minimum energies in the S_{II} and W sites: 27.6 kJ/mol.

$\exp(37.4\ \text{kJ mol}^{-1}/k_B T)$, thus compensating for the Arrhenius behavior that is apparent in Figure 4a.

Transition state theory results for both TS's are very similar, and mainly show an Arrhenius-type behavior reflecting the high energy barrier to the $S_{II} \rightarrow S_{II}$ jump. The activation energies indeed change by no more than 0.7 kJ mol^{-1} between TS's 1 and 2: 37.4 vs 36.7 kJ mol^{-1}, respectively. The prefactor remains approximately the same: 1.6 vs 1.4 $\times 10^{13}$ s^{-1}, respectively. Although these differences are rather small, they are statistically meaningful, as can be seen on Figure 4b.

When dynamical corrections are included, the data obtained with both TS 1 and TS 2 become statistically identical, thus showing the independence with the exact location of the TS of the dynamical rate constant and validating the method used.

The TST values are rather good first approximations to the corrected rate constants. This shows that, if a good initial guess for the transition state dividing surface can be made, the TST calculation provides a very reasonable estimation of the rate constants. This remark is rather important, since the TST calculation is about 6 times more rapid than the complete dynamical calculation for this system.

3. The complete dynamical factors $f_{ij}(t)$ were computed from averaging over 2 000 10 ps runs at 298 K, and are presented in Figure 5. Note that the initial rise of $f(t)$ is an artifact of the calculation, due to the fact that the TS dividing surface considered has a certain ''size'' ϵ, set in this calculation to 0.2 Å. The behavior of $f_{ij}(t)$ agrees well with what was expected and been described in the literature: after an initial rapid decay, $f_{ij}(t)$ reaches an interval where it decays very slowly, down to a plateau. The plateau value is very close to the value obtained from the truncated dynamics, where the runs are stopped as soon as a product site has been reached: 0.735 vs 0.687, and remains within the statistical accuracy of the calculation, estimated here to 0.045 for each value. However, the truncated run takes about 10 times less computing time to complete than the 10 ps run, and therefore all dynamical corrections given hereafter have been computed using truncated dynamic runs. One can see that the possible multisite jumps are very rare, and therefore have been completely neglected in what follows.

IV. RESULTS AND DISCUSSION

A. Chemical equilibrium

The chemical equilibrium constant $\kappa(S_{II} \rightarrow W)$ describes the relative proportion of molecules at W and S_{II} sites. Since there are twice more S_{II} than W sites, what we calculate is the chemical equilibrium constant for one of each site:

$$\kappa^0(S_{II} \rightarrow W) = \frac{1}{2}\kappa(S_{II} \rightarrow W) = \frac{Q(W)}{Q(S_{II})}. \tag{18}$$

This quantity can be computed directly using Voter's displacement vector method described in Section II B. The computations were performed between 80 and 800 K using a bias potential of -28.9 kJ mol^{-1} (close to the difference of the energy minima in the two sites: 27.6 kJ mol^{-1}, as determined by energy minimization), and are presented in Figure 6a and b. The average in both sites is computed over 200 000 Monte Carlo steps. Figure 6a displays the ''raw'' results, while the points in Figure 6b were multiplied by $\exp(27.6\ \text{kJ mol}^{-1}/k_B T)$, so as to scale them and to make apparent the preexponential factor of this typical Arrhenius behavior. For low temperatures (up to 400 K) the prefactor remains constant, reflecting classical harmonic vibrations, and approximately equals 5. When the temperature increases above 400

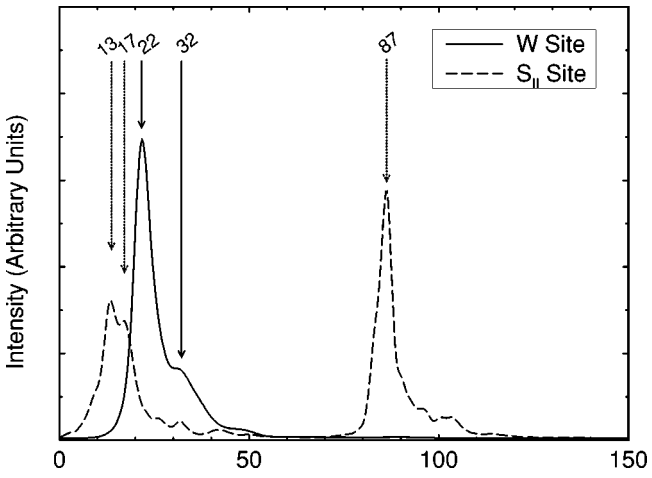

FIG. 7. Vibrational density-of-state of the center-of-mass of benzene in a model of NaY, calculated from two 200 ps MD runs in the NVE ensemble at 298 K. The framework atoms were held fixed during the MD runs. Solid line: Window site. Dotted line: S_{II} site.

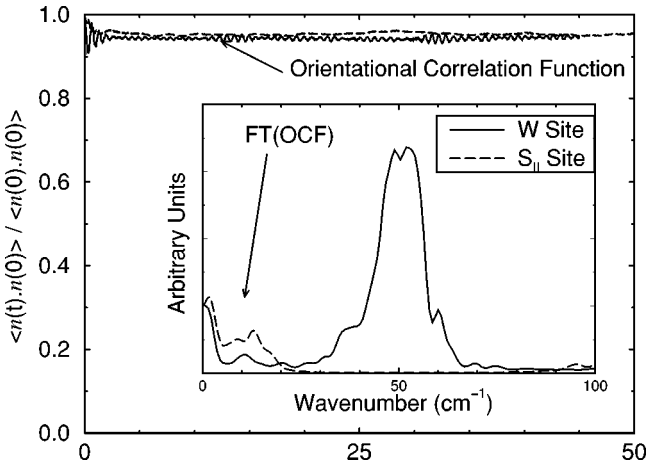

FIG. 8. Orientational correlation function of a vector normal to the benzene plane, calculated from two 200 ps MD runs in the NVE ensemble at 298 K. The framework atoms were held fixed during the MD runs. In inclusion is the Fourier transform of the OCF (shifted to zero so as to hide the baseline). Solid line: Window site. Dotted line: S_{II} site.

K, a slight but significant deviation from strict Arrhenius behavior appears, reflecting anharmonicity, as the apparent prefactor increases up to ≈ 9 for 900 K. Thus entropy effects at low temperature favors the window sites by a factor of 5, as compared to what could be expected from energetic results only, and this favoring increases with temperature.

The difference between adsorption in the S_{II} and W sites may change the rotational, translational, and vibrational molecular partition functions; it is assumed here and in the following that the internal vibrations of benzene do not change between the two states ''sorbed in the S_{II} site'' and ''sorbed in the W site.'' This assumption is quite crude, since it has been shown experimentally that a vibrational shift indeed occurs.[3] However the present Monte Carlo calculation assumes the benzene molecule to be rigid, and therefore the observed partition functions indeed do not account for the shift of the vibrational frequencies. A qualitative estimate of the change undergone by the vibrational and rotational partition functions may be obtained by a thorough analysis of molecular dynamics trajectories in the S_{II} and W sites. Indeed, the strong adsorption transforms the translational and some rotational degrees of freedom into external librations, apparent on the vibrational and orientational density-of-states (see Sec. II B), while the rotational relaxation is given by the decay of the orientational correlation function. The Fourier transform of the latter quantity also shows the frequency of the librations of the sorbed benzene molecules.

Figure 7 presents the vibrational DOS, in the W site (solid line) and in the S_{II} site (dotted line). The external vibrations are significantly different in these two sites. In the W site two low frequencies are apparent, at 22 and 32 cm^{-1}, while in the S_{II} site two low frequencies at ca. 13 and 17 cm^{-1} are followed by a high frequency peak at ca. 87 cm^{-1}. This peak can be attributed unambiguously to the vibration away from the Na cation, while the two nearly degenerated low frequency peaks correspond to the perpendicular vibrations. In the W site, all center-of-mass motions are low frequency motions.

Figure 8 presents the orientational correlation function and, in inclusion, its Fourier transform. One notes, both in the W and S_{II} sites, almost no rotational relaxation during the 50 ps observation window, indicating that at 298 K the molecular axis remains approximately fixed in both adsorption sites. The FT of the OCF shows, however, a medium frequency (50 cm^{-1}) vibration in the Window site but only very low frequency components (<20 cm^{-1}) in the S_{II} site.

There is a clear parallel between the external motions in the Window and S_{II} sites: in both cases, one observes mainly low frequency motions except for one, corresponding to a libration in the W site and an external vibration in the S_{II} site. Hence, there is qualitatively no difference between the entropic contributions to the molecular partition functions in the W and S_{II} sites. Although the overall larger ''stiffness'' of the motions at the S_{II} site, as compared to the motions at the W site, indicate that the preexponential factor of $\kappa^0(S_{II} \rightarrow W)$ should be larger than one, a quantitative estimate of the prefactor requires a complete Monte Carlo calculation: it is a complex function of the molecular motions at the sites.

B. Rate constants

Figure 9 summarizes the rate constants computed between 150 and 500 K for the four jumps $S_{II} \rightarrow S_{II}$, $S_{II} \rightarrow W$, $W \rightarrow S_{II}$, and $W \rightarrow W$, both from TST and TST with dynamical corrections. All Monte Carlo averages were computed over 200 000 MC steps, using bias potentials of -35.6, -43.3, -15.4, and -9.6 kJ mol^{-1} for the $S_{II} \rightarrow S_{II}$, $S_{II} \rightarrow W$, $W \rightarrow S_{II}$ jumps, and $W \rightarrow W$, respectively. The dynamical correction factors were averaged over 2 000 independent MD runs originating on the dividing surface for the first three processes. For the $W \rightarrow W$ jump, more than 10 000 MD runs were performed for each temperature.

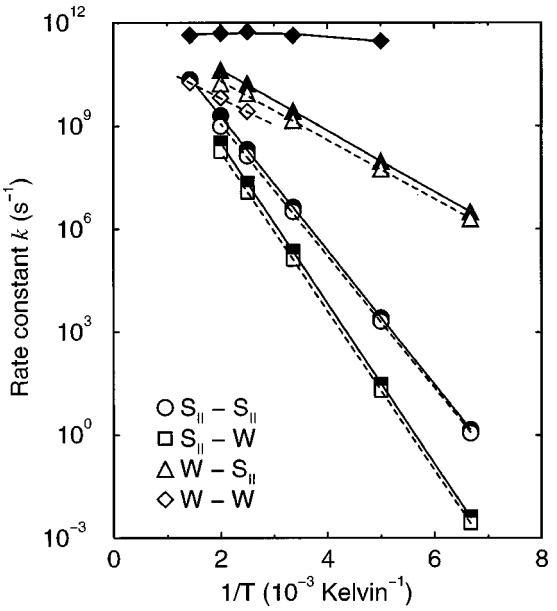

FIG. 9. Plot of the rate constants for a $S_{II} \rightarrow S_{II}$, $S_{II} \rightarrow W$, $W \rightarrow S_{II}$, and $W \rightarrow W$ jumps, using transition state theory (filled symbols) and correlation function theory (open symbols). The lines are a least-square fit of the data points.

An Arrhenius behavior is apparent from the transition state theory rate constants (indicated by filled symbols in Figure 9) for the three processes $S_{II} \rightarrow S_{II}$, $S_{II} \rightarrow W$, and $W \rightarrow S_{II}$. On the other hand, the behavior of $k^{TST}(W \rightarrow W)$ demonstrates practically no activation energy. This is because the $W \rightarrow W$ MEP requires benzene to jump through a narrow transition state region with certain orientations so as not to plummet into a S_{II} site. These complex constraints on the $W \rightarrow W$ dividing surface are not taken into account here, so that many of the states contributing to the $W \rightarrow W$ transition state partition function would fall into a S_{II} site. The negligible activation energy of $k^{TST}(W \rightarrow W)$ reflects the fact that the transition state configurations on the wrong MEP are being counted.

The dynamical corrections do not change much the rate constants for the three processes $S_{II} \rightarrow S_{II}$, $S_{II} \rightarrow W$, and $W \rightarrow S_{II}$. The processes remain Arrhenius-type, with activation energies that agree well with the minimum energy in the sites and at the transition states as previously determined by energy minimisation[5] (see Table I). The dynamical corrections correct much more the preexponential factor than the activation energy itself; indeed, transition state theory in these cases gives a very good first approximation to the rate constants.

The dynamical correction, on the other hand, changes dramatically the rate constant for the $W \rightarrow W$ jump. Indeed, we observe Arrhenius behavior for temperatures of 400 K and above, with an activation of approximately 15 kJ mol^{-1}, close to the energy of the MEP. The dynamical corrections count up only those initial configurations which end up in the requested final state. It was found that the overwhelming majority of the initial configurations found on the W–W ''dividing surface,'' as defined in Sec. II C, end in one of the neighbouring S_{II} site. At high temperature, a certain part of the molecules initially at the ''dividing surface'' do end in the final W site. This part decreases as the temperature decreases, reflecting the observed activation energy of ca. 15 kJ mol^{-1}. For temperatures under 298 K, less than 1 run in 1 000 reacts to a W site, so that even with 10 000 dynamical trajectories no averaged dynamical correction factor could be computed.

Transition state theory is seen to fail qualitatively for the $W \rightarrow W$ jump, using the dividing surface presented in Sec. II C. We have noted in Sec. II B that the dynamical corrections correct mainly, in our case, for the incomplete knowledge of the exact dividing surface. This idea suggests that a different choice of the dividing surface could lead to qualitative agreement between TST and correlation function theory. Since the $W \rightarrow W$ MEP consists of a skateboard motion, with a transition state parallel to the 4-ring plane,[5] it seemed logical to add an orientational constraint on the dividing surface, by imposing the benzene plane to be parallel to the zeolitic 4-ring. However, this choice of dividing surface, as well as other tested orientational constraints, did not lead to any agreement between TST and CF. This points out a general condition when TST will fail: when trajectories on a dividing surface can relax to multiple different product sites, TST can only give an estimate of the total rate out of a site, and cannot give a site-to-site rate.

The preexponential factors for all processes are listed in Table I. As noted before, the dynamical corrections tends to decrease these prefactors by a factor of 1.5 to 2, approximately. Both jumps starting at the S_{II} site present the same preexponential factor, close to 10^{13} s^{-1} (although the activation energy, and the transition state, are different), while for the $W \rightarrow S_{II}$ jump it is much lower: ca. 0.16×10^{13} s^{-1}. These values are in very good agreement with available experimental data on this or similar systems.[8,36,37]

An estimate of the preexponential factor is given by the vibrational frequency in the initial site of the molecular motions along the reaction coordinate, neglecting entropy effects. This leads to $\approx 0.26 \times 10^{13}$ s^{-1} in the S_{II} site (87 cm^{-1}) and between 0.09 and 0.15×10^{13} s^{-1} in the W site (30–50 cm^{-1}). Comparison with the calculated values shows that entropy effects favor strongly the transition state for both jumps originating at the S_{II} site by a factor of 4, but only weakly for the jump from the W site.

The prefactor for the $W \rightarrow W$ jump is lower than for all other processes: ca. 0.024×10^{13} s^{-1}, that is, roughly 7 times less than for the $W \rightarrow S_{II}$ jump, and 50 times less than for the jumps originating at the S_{II} sites. Clearly, entropy effects in this case strongly disfavor this process. This reflects the fact that the W-W MEP is very localized in multidimensional configuration space; that we were able to compute the $W \rightarrow W$ rate constants is a great success of correlation function theory, and of our current implementation.

Detailed balance implies that: $\kappa^0(S_{II} \rightarrow W) = k(S_{II} \rightarrow W)/k(W \rightarrow S_{II})$ The perfect agreement, within statistical accuracy, between the chemical equilibrium constant and the ratio of the rate constants is shown on Figure 10, for the rate constants calculated both by TST and corrected TST (noted

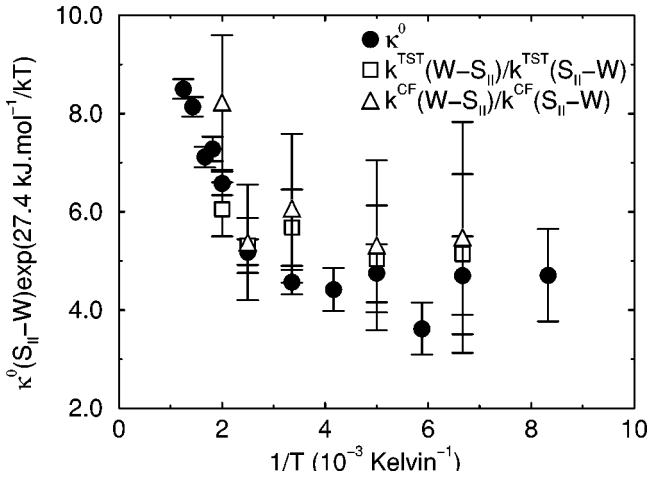

FIG. 10. Chemical equilibrium constants $\kappa^0(S_{II}\rightarrow W)$ (filled circles) and ratio of the rate constants $k(S_{II}\rightarrow W)/k(W\rightarrow S_{II})$, for the rate constants computed by TST (open squares) and correlation function theory (open triangles). The data are compensated for the energy difference between the minimum energy in the S_{II} and W site: 37.4 kJ/mol. Note the very good agreement, within statistical accuracy.

CF for correlation function). Figure 10 presents data corrected for Arrhenius behavior (as presented in Figure 6b), since the uncompensated data appear to overlap exactly. This agreement further confirms the adequacy of the methodology used in this paper for calculating rate constants for benzene in faujasite.

In a general way, the rate constants for benzene hopping in NaY, calculated using correlation function theory, show a definite Arrhenius behavior between 150 and 500 K. The activation energies agree well with the difference between the minimum energies in the initial sites and the transition states. The preexponential factors reflect ''reasonable'' frequencies around $10^{12}-10^{13}$ s^{-1} for all jumps. We note an entropic favoring of the W site as compared to the S_{II} site of a factor of 5 at low temperature up to ca. 9 at high temperature, and correspondingly a favoring of the jumps originating at the S_{II} site as compared to the jumps originating at the W site.

Although the W→W jump presents an activation energy similar to the W→S_{II} jump, the observed prefactor is approximately 10 times smaller (for temperatures above 400 K). Auerbach[6] recently reported an analytical expression for the rate coefficient k for benzene cage-to-cage motion in NaY at infinite dilution:

$$k = k(S_{II}\rightarrow W)\frac{3}{2}\left[1+\frac{k(W\rightarrow W)}{k(W\rightarrow S_{II})}\right]. \tag{19}$$

For temperatures above 400 K, and probably for lower temperatures also, if the Arrhenius behavior of the W→W rate constant can be extended, the ratio $k(W\rightarrow W)/k(W\rightarrow S_{II})$ will remain much smaller than one; hence, the second term of equation 19 will not be important, and the diffusion at infinite dilution clearly will almost exclusively depend on the $S_{II}\rightarrow W$ rate constant. Note, however, that at finite loading this pictures is likely to change, as the W→W jump gains importance due to the blocking of the S_{II} sites.[13]

Similarly, the $S_{II}\rightarrow S_{II}$ process should make up for the temperature dependence of the benzene orientational randomization.[10] These findings are consistent with the available experimental data.[8]

Although this study clearly demonstrates the usefulness of the approach presented and therefore justifies further use of the same methodology, we should note that two features have been excluded from the calculation, which are likely to have a major influence on the rate constants: the benzene internal motions, which may significantly change the Arrhenius prefactors, and the framework motions. Indeed, a preliminary study has shown that inclusion of the motions of the sodium ions could lower the energy barrier to the $S_{II}\rightarrow S_{II}$ jump by ca. 5 kJ mol^{-1}, while the coupling between the vibrations of the sodium ion and the benzene molecule in the S_{II} site is likely to significantly alter the vibration frequency of the latter, thus changing the preexponential factor. It seems necessary, therefore, to perform more simulations including these effects. Furthermore, the orders-of-magnitude difference between the apparent prefactors deduced from NMR measurements between NaY and HY, noted in the introduction, can only stem from a coupling between the molecule's external motions and the framework vibrations, thus emphasizing the need for inclusion of these vibrations.

V. CONCLUSION

We have presented results of transition state theory and correlation function theory calculations of the rate constants for the jumps of one benzene molecule inside a cage of a model NaY zeolite. Transition theory rate constants were computed using the displacement vector method proposed by Voter,[31] while the correlation function calculations followed the formalism of Voter and Doll.[19] This is the first calculation of exact flux correlation function rate coefficients for the motion of non-spherical molecule inside a zeolite framework. Therefore, the study presented in this paper is aimed mainly at establishing and verifying the methods and their application in this complex case.

While the transition state rate constants are dependent on the location of the dividing surface, the correlation function rate constants were shown to be independent of the dividing surface location, provided there is a good enough initial guess. We verified this fact using two different transition states for the $S_{II}\rightarrow S_{II}$ jump. The transition state theory rate constants were found to constitute fair approximations to the more correct correlation function theory rate constants for most of the processes; in the case of the W→W jump, however, transition state theory rate constants proved to be even qualitatively wrong.

The chemical equilibrium coefficient between the S_{II} and W site, as well as the $S_{II}\rightarrow S_{II}$, $S_{II}\rightarrow W$, and $W\rightarrow S_{II}$ rate constants, show an overall Arrhenius behavior between 150 and 500 K. The activation energies agree rather well with the difference between the minimum energies in the initial site and at the transition state. The order of magnitude of the prefactors reflects reasonable external frequencies with values around $10^{12}-10^{13}$ s^{-1}, in good qualitative agreement

with experiment.[8,36,37] The two jumps originating at a S_{II} site present the same prefactor $\approx 10^{13}\ s^{-1}$. This factor is approximately 4 to 5 times larger than the external frequency of the molecular center-of-mass away from the cation, as determined by molecular dynamics. This shows that entropic effects favor the transition state, as compared to the S_{II} site. The prefactor for the $W \rightarrow S_{II}$ jump is much lower: $\approx 0.16 \times 10^{13}\ s^{-1}$. Two effects contribute to this lower prefactor: the smaller external vibration frequency in the window site as compared to the S_{II} site, and almost no entropic favoring of the transition state as compared to the site.

The $W \rightarrow W$ rate constant presents an activation energy similar to the $W \rightarrow S_{II}$ rate constant, but with a much smaller prefactor. The smaller prefactor originates in the complicated and rather unstable minimum energy path from one window to another. In the range of temperatures studied here, and for infinite dilution, the $S_{II} \rightarrow W$ process clearly constitutes the limiting process for benzene intercage diffusion.

This study demonstrates the efficacy of the approach used to compute rate constants for the diffusion of nonspherical molecules in zeolites. However, we left out two important aspects of the molecular motions, which are likely to influence the rate constants: benzene internal motions, and framework motions. A complete analysis of the rate constants for benzene diffusion in NaY, and a meaningful comparison with USY and HY, needs take into account these motions. These issues will be addressed in a forthcoming publication.

ACKNOWLEDGMENTS

S.M.A. acknowledges support from the NSF under Grants Nos. CHE-9625735 and CHE-9616019, and from Molecular Simulations, Inc. for generously providing visualization software.

[1] B. L. Su and D. Barthomeuf, J. Catal. **139**, 81 (1993).
[2] B. L. Su and D. Barthomeuf, Appl. Catal. A: General **124**, 81 (1995).
[3] B. L. Su, J. Chem. Soc. Faraday Trans. **97**, 1449 (1997).
[4] P. J. O'Malley and C. J. Braithwaite, Zeolite **15**, 198 (1995).
[5] S. M. Auerbach, N. J. Henson, A. K. Cheetham, and H. I. Metiu, J. Phys. Chem. **99**, 10600 (1995).
[6] S. M. Auerbach, L. M. Bull, N. J. Henson, H. I. Metiu, and A. K. Cheetham, J. Phys. Chem. **100**, 5923 (1996).
[7] P. Demontis, S. Yashonath, and M. L. Klein, J. Phys. Chem. **93**, 5016 (1989).
[8] J. A. Sousa Gonçalves, R. L. Portsmouth, P. Alexander, and L. F. Gladden, J. Phys. Chem. **99**, 3317 (1995).
[9] H. Klein, H. Fuess, and G. Schrimpf, J. Phys. Chem. **100**, 11101 (1996).
[10] S. M. Auerbach and H. I. Metiu, J. Chem. Phys. **105**, 3753 (1996).
[11] S. M. Auerbach and H. I. Metiu, J. Chem. Phys. **106**, 2893 (1997).
[12] S. M. Auerbach, J. Chem. Phys. **106**, 7810 (1997).
[13] C. Saravanan and S. M. Auerbach, J. Chem. Phys. (accepted for publication).
[14] A. N. Fitch, H. Jobic, and A. Renouprez, J. Phys. Chem. **90**, 1311 (1986).
[15] M. Czjzek, H. Jobic, A. N. Fitch, and T. Vogt, J. Phys. Chem. **96**, 1535 (1992).
[16] R. L. June, A. T. Bell, and D. N. Theodorou, J. Phys. Chem. **95**, 8866 (1991).
[17] A. F. Voter and J. D. Doll, J. Chem. Phys. **80**, 5832 (1984).
[18] D. G. Truhlar, B. C. Garett, and S. J. Klippenstein, J. Phys. Chem. **100**, 12771 (1996).
[19] A. F. Voter and J. D. Doll, J. Chem. Phys. **82**, 80 (1985).
[20] Z. Zhang, K. Haug, and H. Metiu, J. Chem. Phys. **93**, 3614 (1990).
[21] T. Mosell, G. Schrimpf, C. Hahn, and J. Brickmann, J. Phys. Chem. **100**, 4571 (1996); T. Mosell, G. Schrimpf, and J. Brickmann, J. Phys. Chem. **100**, 4582 (1996).
[22] R. Q. Snurr, A. T. Bell, and D. N. Theodorou, J. Phys. Chem. **98**, 11948 (1994).
[23] E. J. Maginn, A. T. Bell, and D. N. Theodorou, J. Phys. Chem. **100**, 7155 (1996).
[24] F. Jousse, L. Leherte, and D. P. Vercauteren, J. Phys. Chem. B **101**, 4717 (1997).
[25] L. Greengard and V. Rokhlin, J. Comput. Phys. **73**, 325 (1987).
[26] H. Y. Wang and R. LeSar, J. Chem. Phys. **104**, 4173 (1996).
[27] C. A. White and M. Head-Gordon, J. Chem. Phys. **101**, 6593 (1994).
[28] H. G. Petersen, D. Soelvason, J. W. Perram, and E. R. Smith, J. Chem. Phys. **101**, 8870 (1994).
[29] K. E. Schmidt and M. A. Lee, J. Stat. Phys. **63**, 1223 (1991).
[30] D. Chandler, J. Chem. Phys. **68**, 2959 (1978).
[31] A. F. Voter, J. Chem. Phys. **82**, 1890 (1985).
[32] G. Hummer and A. Szabo, J. Chem. Phys. **105**, 2004 (1996).
[33] P. V. Kumar, J. S. Raut, S. J. Warakomski, and K. A. Fichthorn, J. Chem. Phys. **105**, 686 (1996).
[34] S. Kumar, P. W. Wayne, and M. Vásquez, J. Comput. Chem. **17**, 1269 (1996).
[35] M. P. Allen and D. J. Tildesley, *Computer Simulations of Liquids* (Clarendon, Oxford, 1987).
[36] R. Burmeister, H. Schwarz, and B. Boddenberg, Ber. Bunsenges. Phys. Chem. **93**, 1309 (1989).
[37] L. M. Bull, N. J. Henson, A. K. Cheetham, J. M. Newsam, and S. J. Heyes, J. Phys. Chem. **97**, 11776 (1993).